PHYSICAL REVIEW D **90,** 095009 (2014)

Higgs precision analysis updates 2014

Kingman Cheung,[1,2,*] Jae Sik Lee,[3,†] and Po-Yan Tseng[1,‡]

[1]*Department of Physics, National Tsing Hua University, Hsinchu 300, Taiwan*

[2]*Division of Quantum Phases and Devices, School of Physics, Konkuk University, Seoul 143-701, Republic of Korea*

[3]*Department of Physics, Chonnam National University, 300 Yongbong-dong, Buk-gu, Gwangju 500-757, Republic of Korea*

(Received 12 August 2014; published 12 November 2014)

During the 2014 summer conferences, both the ATLAS and CMS Collaborations of the LHC experiments have demonstrated tremendous efforts in treatment of data and processing more data such that most data on signal strengths have improved, especially the diphoton and fermionic modes of both experiments. Here in this paper we perform an update to our previous model-independent Higgs precision analysis—Higgcision. We found the following: (i) the uncertainties on most couplings shrink about 10%–20%, (ii) the nonstandard (e.g. invisible) decay branching ratio of the Higgs boson is constrained to be less than 19% if only the width is allowed to vary, (iii) the gauge-Higgs coupling C_v is constrained to be $0.94^{+0.11}_{-0.12}$, in which the uncertainty is reduced by about 10%, and (iv) the standard model (SM) Higgs boson still provides the best fit to all the Higgs boson data, and compared to the previous results the SM Higgs boson now enjoys a higher p value than the last year.

DOI: 10.1103/PhysRevD.90.095009 PACS numbers: 14.80.Bn, 14.80.Ec

I. INTRODUCTION

It has been two years since a new particle was discovered at the Large Hadron Collider (LHC) [1,2]. The initial data sets indicated that it might be different from the standard model (SM) Higgs boson. Nevertheless, after two more years of collecting data and more painful scrutinizing of the uncertainties and handling the backgrounds, the data showed that it is more and more likely to be the SM Higgs boson. Indeed, we showed in Ref. [3] that the SM Higgs boson provided the best fit to all the Higgs-boson data after the summer 2013 conference. Similar results were obtained in a number of model-independent studies after the summer 2013 conference [4].

Most new Higgs boson results with improvements were presented in the ICHEP 2014 [5,6]. In particular, the signal strength of the diphoton decay channel of ATLAS has changed from 1.6 ± 0.4 to 1.17 ± 0.27 [7] and that of CMS from $0.78^{+0.28}_{-0.16}$ to $1.12^{+0.37}_{-0.32}$ [8]. Also, some updates were reported in the ZZ [9,10], the WW [11,12], $b\bar{b}$ [13], and $\tau^+\tau^-$ [14] decay modes, as well as the $t\bar{t}H$ events [15,16] since 2013. There was also an overall update from the DØ [17]. Here in this paper we present an update to our previous model-independent Higgs precision analysis—Higgcision [3].

The organization of the paper is as follows. In the next section, we list all the improved Higgs boson data used in our global fits and the updated fitting results are presented in Sec. III. We conclude in Sec. IV.

*cheung@phys.nthu.edu.tw
†jslee@jnu.ac.kr
‡d9722809@oz.nthu.edu.tw

II. HIGGS SIGNAL STRENGTH DATA

The updated data on Higgs signal strengths are tabulated in Tables I–V. We describe the notable differences between the current data set and the one in summer 2013.

(i) $H \to \gamma\gamma$ has the most significant changes since the summer 2013 conference. The ATLAS Collaboration updated their best-measured value $\mu_{ggH+ttH} = 1.6 \pm 0.4$ [18] to $\mu_{\text{inclusive}} = 1.17 \pm 0.27$ [7]. The χ^2_{SM} for the ATLAS $H \to \gamma\gamma$ channel reduces from 3.2 to 0.96. This data is now brought closer to the SM value.

(ii) The CMS $H \to \gamma\gamma$ data also entertain a dramatic change. It was the $\mu_{\text{untagged}} = 0.78^{+0.28}_{-0.26}$ [19], and now it becomes $\mu_{ggH} = 1.12^{+0.37}_{-0.32}$ [8], which is now the most significant one among the μ's for the diphoton channel. The underlying reason is believed to be better modeling of the diphoton background and calibration of the photons. The data are also brought closer to the SM value.

(iii) The ATLAS $H \to ZZ^*$ data increase from 1.5 ± 0.4 [20] to $1.66^{+0.45}_{-0.38}$ [9], such that the χ^2_{SM} jumps from 1.6 to 3.0. The CMS $H \to ZZ^*$ stays about the same [10,21]. The ZZ^* channel becomes more important in the overall fitting.

(iv) The CMS $H \to WW^*$ data show some improvements [12,22]. While the μ (0/1 jet) stays about the same, the μ_{VBF} and μ_{VH} show positive central values now. Also, a new $\mu_{WH}(3\ell 3\nu)$ is now available. The ATLAS $H \to WW^*$ remains the same [11,20].

(v) Both ATLAS and CMS show improvements in the $H \to b\bar{b}$ channel because a close-to-full set of data

TABLE I. Data on signal strengths of $H \to \gamma\gamma$ by the ATLAS and CMS, and at the Tevatron after ICHEP 2014. The luminosity updates at 8 TeV are shown in the parentheses. The percentages of each production mode in each data row are given. The χ^2 of each data with respect to the SM is shown in the last column. The subtotal χ^2 of this decay mode is shown at the end.

	Signal strength μ	M_H (GeV)	Production mode				
Channel	c.v $\pm$ error		ggF	VBF	VH	ttH	$\chi^2_{\rm SM}$ (each)
	ATLAS (4.5 fb^{-1} at 7 TeV + 20.3 fb^{-1} at 8 TeV): p. 29 of [7] (Aug. 2014)						
μ_{ggH}	1.32 ± 0.38	125.40	100%	-	-	-	0.71
μ_{VBF}	0.8 ± 0.7	125.40	-	100%	-	-	0.08
μ_{WH}	1.0 ± 1.6	125.40	-	-	100%	-	0.00
μ_{ZH}	$0.1^{+3.7}_{-0.1}$	125.40	-	-	100%	-	0.06
μ_{ttH}	$1.6^{+2.7}_{-1.8}$	125.40	-	-	-	100%	0.11
	CMS (5.1 fb^{-1} at 7 TeV + 19.7 fb^{-1} at 8 TeV): Fig. 24 of [8] (July 2014)						
μ_{ggH}	$1.12^{+0.37}_{-0.32}$	124.70	100%	-	-	-	0.14
μ_{VBF}	$1.58^{+0.77}_{-0.68}$	124.70	-	100%	-	-	0.73
μ_{VH}	$-0.16^{+1.16}_{-0.79}$	124.70	-	-	100%	-	1.00
μ_{ttH}	$2.69^{+2.51}_{-1.81}$	124.70	-	-	-	100%	0.87
	Tevatron (10.0 fb^{-1} at 1.96 TeV): p. 32 of [25] (Nov. 2012)						
Combined	$6.14^{+3.25}_{-3.19}$	125	78%	5%	17%	-	2.60
							subtotal: 6.30

was analyzed. Both show the VH tag and ttH tag results [13,15,23]. See Table IV.

(vi) The ATLAS $H \to \tau\tau$ channel has analyzed the full set of data and shows some improvements: both central values are close to 1 and the size of the errors is reduced [24]. The CMS now separately reported 0-jet and 1-jet categories. The size of errors slightly improves [14].

(vii) The deviations from the SM for each Higgs decay channel in terms of $\chi^2_{\rm SM}$ are listed in the last column

TABLE II. The same as Table I but for $H \to ZZ^{(*)}$.

	signal strength μ	M_H (GeV)	Production mode				
Channel	c.v $\pm$ error		ggF	VBF	VH	ttH	$\chi^2_{\rm SM}$ (each)
	ATLAS (4.5 fb^{-1} at 7 TeV + 20.3 fb^{-1} at 8 TeV): page 18 of [9] (June 2014), page 18 of [5]						
Inclusive	$1.66^{+0.45}_{-0.38}$	124.51	87.5%	7.1%	4.9%	0.5%	3.02
	CMS (5.1 fb^{-1} at 7 TeV + 19.7 fb^{-1} at 8 TeV): abstract of [10] (Dec. 2013)						
Inclusive	$0.93^{+0.29}_{-0.25}$	125.6	87.5%	7.1%	4.9%	0.5%	0.06
							subtotal: 3.07

TABLE III. The same as Table I but for $H \to WW^{(*)}$.

	Signal strength μ	M_H (GeV)	Production mode				
Channel	c.v $\pm$ error		ggF	VBF	VH	ttH	$\chi^2_{\rm SM}$ (each)
	ATLAS (4.6 fb^{-1} at 7 TeV + 20.7 fb^{-1} at 8 TeV): page 10 of [11] (July 2014)						
Inclusive	0.99 ± 0.30	125	87.5%	7.1%	4.9%	0.5%	0.00
	CMS (4.9 fb^{-1} at 7 TeV + 19.4 fb^{-1} at 8 TeV): Fig. 23 of [12] (Dec. 2013)						
0/1 jet	$0.74^{+0.22}_{-0.20}$	125.6	97%	3%	-	-	1.40
VBF tag	$0.60^{+0.57}_{-0.46}$	125.6	17%	83%	-	-	0.49
VH tag ($2l2\nu2j$)	$0.39^{+1.97}_{-1.87}$	125.6	-	-	100%	-	0.10
WH tag ($3l3\nu$)	$0.56^{+1.27}_{-0.95}$	125.6	-	-	100%	-	0.12
	Tevatron (10.0 fb^{-1} at 1.96 TeV): p. 32 of [25] (Nov. 2012)						
Combined	$0.85^{+0.88}_{-0.81}$	125	78%	5%	17%	-	0.03
							subtotal: 2.14

TABLE IV. The same as Table I but for $H \to b\bar{b}$.

Channel	signal strength μ c.v $\pm$ error	M_H (GeV)	Production mode ggF	VBF	VH	ttH	$\chi^2_{\rm SM}$ (each)
	ATLAS (4.7(4.5) fb^{-1} at 7 TeV + 20.3 fb^{-1} at 8 TeV): Fig. 19 of [23] (July 2013), p. 18 of [15]						
VH tag	$0.2^{+0.7}_{-0.6}$	125.5	-	-	100%	-	1.31
ttH tag	$1.8^{+1.66}_{-1.57}$	125.4	-	-	-	100%	0.26
	CMS (5.1 fb^{-1} at 7 TeV + 18.9 fb^{-1} at 8 TeV) [13] (Oct. 2013), (19.5 fb^{-1} at 8 TeV)[16] (July 2014)						
VH tag	1.0 ± 0.5	125	-	-	100%	-	0.00
ttH tag	$0.67^{+1.35}_{-1.33}$	125	-	-	-	100%	0.06
	Tevatron (10.0 fb^{-1} at 1.96 TeV): [17]						
VH tag	$1.59^{+0.69}_{-0.72}$	125	-	-	100%	-	0.67
							subtotal: 2.30

TABLE V. The same as Table I but for $H \to \tau\tau$. The correlation for the $\tau\tau$ data of ATLAS is $\rho = -0.51$.

Channel	Signal strength μ	M_H (GeV)	Production mode ggF	VBF	VH	ttH	$\chi^2_{\rm SM}$ (each)
	ATLAS (20.3 fb^{-1} at 8 TeV): p. 28 of [24] (Nov. 2013)						
$\mu(ggF)$	$1.1^{+1.3}_{-1.0}$	125	100%	-	-	-	0.85
$\mu(VBF + VH)$	$1.6^{+0.8}_{-0.7}$	125	-	59.6%	40.4%	-	
	CMS (4.9 fb^{-1} at 7 TeV + 19.7 fb^{-1} at 8 TeV) Fig. 16 of [14] (Jan. 2014)						
0 jet	0.34 ± 1.09	125	96.9%	1.0%	2.1%	-	0.37
1 jet	1.07 ± 0.46	125	75.7%	14.0%	10.3%	-	0.02
VBF tag	0.94 ± 0.41	125	19.6%	80.4%	-	-	0.02
VH tag	-0.33 ± 1.02	125	-	-	100%	-	1.70
							subtotal: 2.96

in Tables I–V. Previously, it is largely dominated by the $\gamma\gamma$ channel but now its significance is somewhat reduced and the ZZ^* becomes more important.

(viii) The total $\chi^2_{\rm SM}$/d.o.f. for the SM is now 16.76/29, compared to the previous one 18.92/22. Substantial improvement for the SM can be seen. The p value for the SM increases from 0.65 to 0.966.

(ix) We also note that the Higgs boson mass measurement at ATLAS now gives $M_H = 125.4 \pm 0.4$ GeV ($H \to \gamma\gamma$) [7] and $124.51 \pm 0.52(\text{stat}) \pm 0.06(\text{syst})$ GeV ($H \to ZZ^*$) [5] with the smaller difference and noticeable improvement on systematics. The corresponding CMS values are $M_H = 124.70 \pm 0.31(\text{stat}) \pm 0.15(\text{syst})$ GeV ($H \to \gamma\gamma$) and $125.6 \pm 0.4(\text{stat}) \pm 0.2(\text{syst})$ GeV ($H \to ZZ^*$) [6]. It is interesting to note that the ATLAS $H \to \gamma\gamma$ ($H \to ZZ^*$) value is similar in size to the CMS $H \to ZZ^*$ ($H \to \gamma\gamma$) one.

III. FITS

The formalism, notation, and convention follow closely our earlier paper [3]. We restate the notation of the coupling parameters that are used here. The normalized Yukawa couplings are

$$C_u^S = g^S_{H\bar{u}u}, \quad C_d^S = g^S_{H\bar{d}d}, \quad C_\ell^S = g^S_{H\bar{l}l}; \quad C_v = g_{HVV};$$
$$C_u^P = g^P_{H\bar{u}u}, \quad C_d^P = g^P_{H\bar{d}d}, \quad C_\ell^P = g^P_{H\bar{l}l}, \tag{1}$$

where the superscripts "S" and "P" denote scalar and pseudoscalar couplings. In the SM, all scalar Yukawa couplings and C_v equal 1, while the pseudoscalar ones equal 0. Here we also assume generation independence and custodial symmetry between the W and Z bosons. In the fits, the deviations due to additional particles running in the triangular loops of the $H\gamma\gamma$ and Hgg vertices are given by

$$\Delta S^\gamma, \quad \Delta P^\gamma; \quad \Delta S^g, \quad \Delta P^g. \tag{2}$$

In the SM, these factors are 0. Finally, the additional contribution to the width of the Higgs boson, $\Delta\Gamma_{\rm tot}$, is also used.

The labeling of the fits is as follows: CPC denotes CP conserving, CPV denotes CP violating, and the number after CPC or CPV denotes the number of varying parameters.

A. CP conserving fits

In the CP conserving fits, we have set all pseudoscalar couplings and form factors to be zero:

$$C^P_{u,d,\ell} = \Delta P^{g,\gamma} = 0, \tag{3}$$

TABLE VI. The best-fit values and the 1σ errors for the parameters in various CP conserving fits and the corresponding chi-square per degree of freedom and the p value after the ICHEP 2014. For the SM, we obtain $\chi^2 = 16.76$, $\chi^2/\text{d.o.f.} = 16.76/29$, and the p value $= 0.966$.

Cases	CPC 1	CPC 2	CPC 3	CPC 4	CPC 6
Parameters	Vary $\Delta\Gamma_{\text{tot}}$	Vary ΔS^γ, ΔS^g	Vary ΔS^γ, ΔS^g, $\Delta\Gamma_{\text{tot}}$	Vary C_u^S, C_d^S, C_ℓ^S, C_v	Vary C_u^S, C_d^S, C_ℓ^S, C_v ΔS^γ, ΔS^g
			After ICHEP 2014		
C_u^S	1	1	1	$0.92^{+0.15}_{-0.13}$	$1.22^{+0.32}_{-0.38}$
C_d^S	1	1	1	$-1.00^{+0.29}_{-0.30}$	$-0.97^{+0.30}_{-0.34}$
C_ℓ^S	1	1	1	$0.99^{+0.17}_{-0.17}$	$1.00^{+0.18}_{-0.17}$
C_v	1	1	1	$0.98^{+0.10}_{-0.11}$	$0.94^{+0.11}_{-0.12}$
ΔS^γ	0	$-0.72^{+0.76}_{-0.74}$	$-0.84^{+0.80}_{-0.82}$	0	$-1.43^{+1.02}_{-0.95}$
ΔS^g	0	$-0.009^{+0.047}_{-0.048}$	$0.02^{+0.10}_{-0.08}$	0	$-0.22^{+0.28}_{-0.24}$
$\Delta\Gamma_{\text{tot}}$ (MeV)	$-0.020^{+0.45}_{-0.37}$	0	$0.39^{+1.13}_{-0.76}$	0	0
χ^2/d.o.f.	16.76/28	15.81/27	15.59/26	16.70/25	14.83/23
p value	0.953	0.956	0.945	0.892	0.901

Cases	CPC N2	CPC N3	CPC N4			
Parameters	Vary C_u^S, C_v	Vary C_u^S, C_v, ΔS^γ	Vary C_u^S, C_v, ΔS^γ, ΔS^g			
			After ICHEP 2014			
C_u^S	$1.017^{+0.092}_{-0.084}$	$1.04^{+0.10}_{-0.089}$	$1.22^{+0.32}_{-0.37}$	$1.22^{+0.32}_{-0.37}$	$-1.22^{+0.37}_{-0.32}$	$-1.22^{+0.37}_{-0.32}$
C_d^S	1	1	1	1	1	1
C_ℓ^S	1	1	1	1	1	1
C_v	$0.993^{+0.062}_{-0.068}$	$0.933^{+0.078}_{-0.082}$	$0.944^{+0.080}_{-0.084}$	$0.944^{+0.080}_{-0.084}$	$0.944^{+0.080}_{-0.084}$	$0.944^{+0.080}_{-0.084}$
ΔS^γ	0	$-1.10^{+0.87}_{-0.81}$	$-1.38^{+1.02}_{-0.94}$	$-1.38^{+1.02}_{-0.94}$	$2.89^{+1.10}_{-1.10}$	$2.89^{+1.11}_{-1.10}$
ΔS^g	0	0	$-0.13^{+0.26}_{-0.22}$	$-1.47^{+0.27}_{-0.24}$	$0.20^{+0.22}_{-0.26}$	$1.55^{+0.24}_{-0.27}$
$\Delta\Gamma_{\text{tot}}$ (MeV)	0	0	0	0	0	0
χ^2/d.o.f.	16.72/27	15.13/26	14.85/25	14.85/25	14.85/25	14.85/25
p value	0.938	0.955	0.945	0.945	0.945	0.945

while varying

$$C_{u,d,\ell}^S, \quad C_v, \quad \Delta S^{g,\gamma}, \quad \Delta\Gamma_{\text{tot}}. \tag{4}$$

1. CPC1: Vary only $\Delta\Gamma_{\text{tot}}$ while keeping $C_u^S = C_d^S = C_\ell^S = C_v = 1$ and $\Delta S^\gamma = \Delta S^g = 0$

The $\Delta\Gamma_{\text{tot}}$ can account for additional decay modes of the observed Higgs boson, in particular the celebrated invisible decay mode into hidden-sector particles, dark matter, etc. The 1-σ-fit value is shown in the second column of Table VI. The variation of chi-square around the minimum chi-square point is shown in Fig. 1. We found that $\Delta\Gamma_{\text{tot}}$ alone does not improve the chi-square and the central value is consistent with 0. The 95% allowed range for $\Delta\Gamma_{\text{tot}}$ is

$$\Delta\Gamma_{\text{tot}} = -0.020^{+0.97}_{-0.66}\ \text{MeV}. \tag{5}$$

Comparing to the previous value $0.10^{+1.11}_{-0.74}$ MeV, the upper error improves by more than 10%. Thus, the 95% C.L. upper limit for $\Delta\Gamma_{\text{tot}}$ improves to 0.97 MeV. Therefore, the nonstandard branching ratio of the Higgs boson is constrained to be

$$B(H \to \text{nonstandard}) < 19\%, \tag{6}$$

which shows a 14% improvement from the previous value of 22%. Note that such a stringent bound can be relaxed when other parameters are allowed to vary in the fits. For

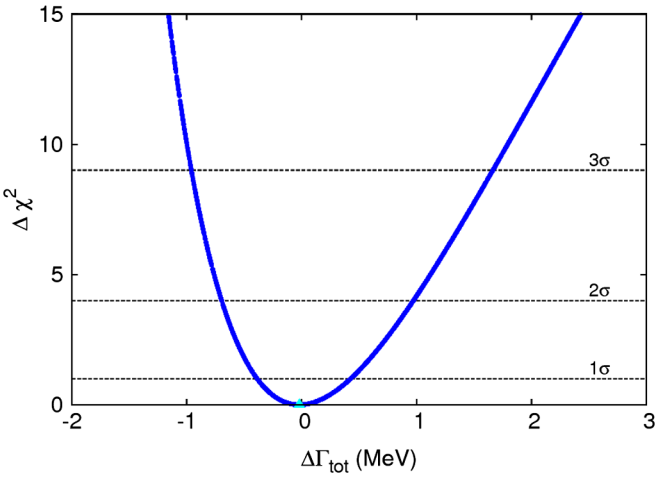

FIG. 1 (color online). Variation of $\Delta\chi^2$ versus $\Delta\Gamma_{\text{tot}}$ in the CPC1 case.

example, in the CPC3 fit below the 1-σ range for $\Delta\Gamma_{\rm tot}$ is $0.39^{+1.13}_{-0.76}$, which can easily translate into a branching ratio of order 50%. This is consistent with a direct search for invisible decay of the Higgs boson [26].

2. CPC2: Vary ΔS^γ and ΔS^g while keeping $C_u^S = C_d^S = C_\ell^S = C_v = 1$

This case can account for additional electrically charged particles or colored particles running in the triangular loops of $H\gamma\gamma$ and Hgg, respectively, while the Yukawa and gauge-boson couplings take on SM values. The best fit value for CPC2 is shown in the third column of Table VI. The central value of $\Delta S^\gamma = -0.72$ is to increase the form factor $S^\gamma_{\rm SM} = -6.64$ [3] by about 11%, while the central value of $\Delta S^g = -0.009$ decreases form factor $S^g_{\rm SM} = 0.64$ by about 1%. Overall, the diphoton rate, which is proportional to $|S^\gamma|^2|S^g|^2$ increases by about 20% so as to match the central values of the ATLAS and CMS data. Although the total chi-square reduced by 1.0 units, the p value of this CPC2 fit is almost the same as the SM p value.

3. CPC3: Vary ΔS^γ, ΔS^g, and $\Delta\Gamma_{\rm tot}$ while keeping $C_u^S = C_d^S = C_\ell^S = C_v = 1$

We have one more varying parameter, $\Delta\Gamma_{\rm tot}$, than the previous case. The central values and uncertainties for ΔS^γ and ΔS^g are similar to the previous case. No improvement from the previous one is seen, as shown in the fourth column of Table VI. The 1-σ range for $\Delta\Gamma_{\rm tot}$ is $0.39^{+1.13}_{-0.76}$ MeV. In this three-parameter fit, the constraint on $\Delta\Gamma^{\rm tot}$ is much relaxed than the CPC1 fit, because of marginalizing the other two parameters. Such a large uncertainty in $\Delta\Gamma_{\rm tot}$ would give a nonstandard decay branching ratio of order $O(50)\%$ for the Higgs boson.

4. CPC4: Vary C_u^S, C_d^S, C_ℓ^S, C_v while keeping $\Delta S^\gamma = \Delta S^g = 0$

In this fit, only the Yukawa and gauge couplings are allowed to vary, which will in turn modify the form factors S^γ and S^g, even though ΔS^γ and ΔS^g are fixed at zero. The result is similar to the one in summer 2013, as shown in the fifth column of Table VI. The gauge coupling is constrained to be $0.98^{+0.10}_{-0.11}$ compared to the previous one at $1.04^{+0.12}_{-0.14}$. We can see some improvement in the uncertainty of order 20%. The uncertainties in Yukawa couplings are about the same.

The sign of the top-Yukawa coupling C_u^S is the most nontrivial one in this case because the coefficients of the W and top contributions to the form factor S^γ come in comparable size but of opposite sign. The top-quark contribution tends to offset parts of the W contribution when $C_u^S > 0$ but enhance when $C_u^S < 0$. Note that the contributions from the bottom quark and tau lepton are relatively much smaller. The result shown in Fig. 3(a) of Ref. [3], as of summer 2013, indicated that positive C_u^S around 0.8 was preferred but around -0.9 was still allowed at 95% C.L. Now we show the corresponding plot based on the most updated data in summer 2014 in Fig. 2. We can see that the value of C_u^S around 0.9 is more preferred than before while the island around -0.9 diminished.

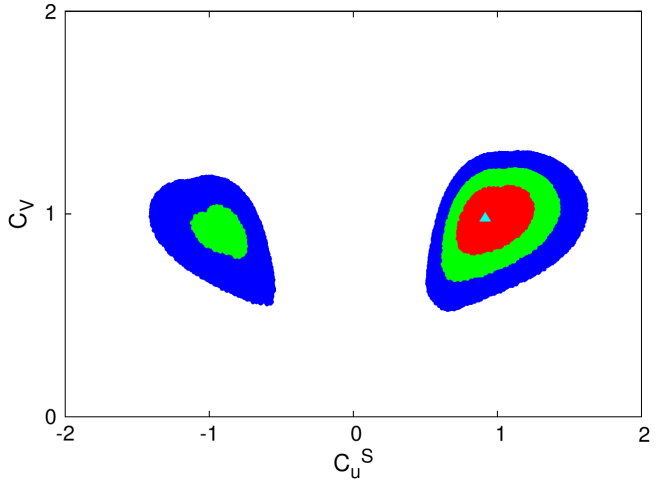

FIG. 2 (color online). The confidence-level regions in the plane of (C_u^S, C_v) of the CPC4 fit by varying C_u^S, C_d^S, C_l^S, and C_v while keeping $\Delta S^\gamma = \Delta S^g = \Delta\Gamma_{\rm tot} = 0$. The contour regions shown are for $\Delta\chi^2 \le 2.3$ (red/gray), 5.99 (green/light gray), and 11.83 (blue/dark gray) above the minimum, which correspond to confidence levels of 68.3%, 95%, and 99.7%, respectively. The best-fit point is denoted by the triangle.

5. CPC6: Vary C_u^S, C_d^S, C_ℓ^S, C_v, ΔS^γ, ΔS^g

This CPC case has the most varying parameters. We found that there are a few sets of degenerate solutions. We first discuss the one with a smaller $|\Delta S^g|$ because the new colored particles are likely to be heavy, and a positive top-Yukawa coupling as a more conventional choice though it is not necessarily the case. The result is shown in the last column of Table VI. Compared to the result in summer 2013 [3], where we have $C_u^S = 0.00 \pm 1.13$, the most notable difference is that the top-Yukawa C_u^S takes on a nonzero value, and correspondingly the ΔS^γ turns negative or positive due to its correlation to C_u^S. Specifically, we observe that the $C_u^S = 0$ hypothesis has been ruled out at 68.3% C.L.

As we have just said, there are a few sets of degenerate solutions. They all give the same chi-square and thus the same p value, as shown in Table IX and Fig. 3. The degenerate solutions arise because the diphoton rate is proportional to $|S^\gamma|^2|S^g|^2$. Numerically, S^γ and S^g are given by [3]

$$S^\gamma \simeq -8.35C_v + 1.76C_u^S + \Delta S^\gamma$$
$$S^g \simeq 0.69C_u^S + \Delta S^g.$$

In Table IX, the value of $C_v = 0.94$. With $|\Delta S^\gamma| \le 4$, four categories of solutions exist for $(C_u^S, \Delta S^\gamma, \Delta S^g) \approx$ $(1.22, -1.4, -0.2)$, $(1.22, -1.4, -1.5)$, $(-1.23, 2.8, 0.2)$,

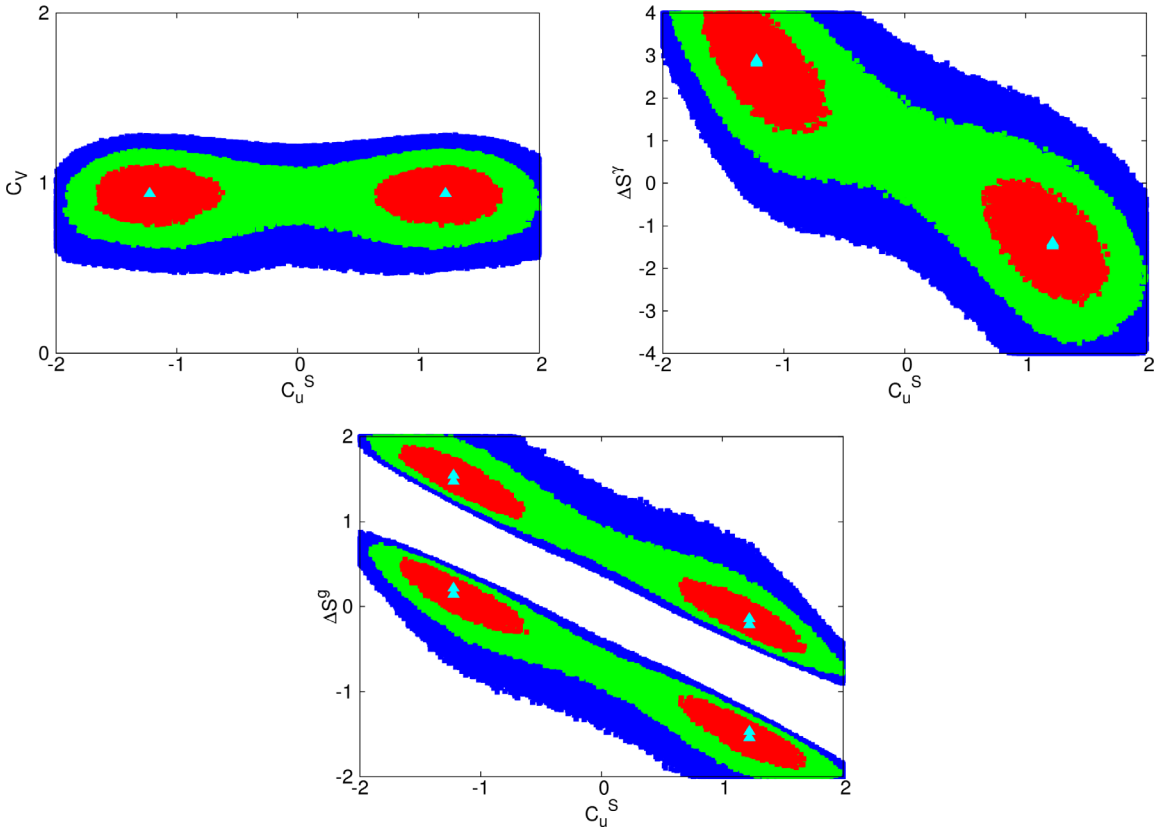

FIG. 3 (color online). The confidence-level regions in the plane of (C_u^S, C_v), $(C_u^S, \Delta S^\gamma)$, and $(C_u^S, \Delta S^g)$ of the CPC6 fit by varying C_u^S, C_d^S, C_l^S, C_v, ΔS^γ, and ΔS^g. The contour regions shown are for $\Delta\chi^2 \leq 2.3$ (red/gray), 5.99 (green/light gray), and 11.83 (blue/dark gray) above the minimum, which correspond to confidence levels of 68.3%, 95%, and 99.7%, respectively. The best-fit points are denoted by the triangles.

$(-1.23, 2.8, 1.5)$. In each category, we find four solutions corresponding to the four combinations of the signs of $C_{d,\ell}^S$.

6. CPC N2: Vary only C_u^S and C_v while keeping others fixed

In all previous CPC fits, we find that the most effective parameters are C_v, C_u^S, and ΔS^γ but less on ΔS^g. We first look at C_u^S and C_v in this special two-parameter fit CPC N2. It is listed in the second column of the lower panel in Table VI. Both C_u^S and C_v are close to the SM values with less than 10% uncertainty.

7. CPC N3: Vary only C_u^S, C_v, and ΔS^γ while keeping others fixed

The result is shown in third column of the lower panel in Table VI, and it is similar to the CPC2 case with C_v and C_u^S close to 1 and ΔS^γ close to -1.

8. CPC N4: Vary only C_u^S, C_v, ΔS^γ, and ΔS^g while keeping others fixed

The result is shown in the last four columns of the lower panel in Table VI, and very similar to that of the CPC6 case. There are four sets of solutions. They have a higher p value than in the CPC6 case since we are taking $C_d^S = C_\ell^S = 1$, which does not much affect our fits to the current data.

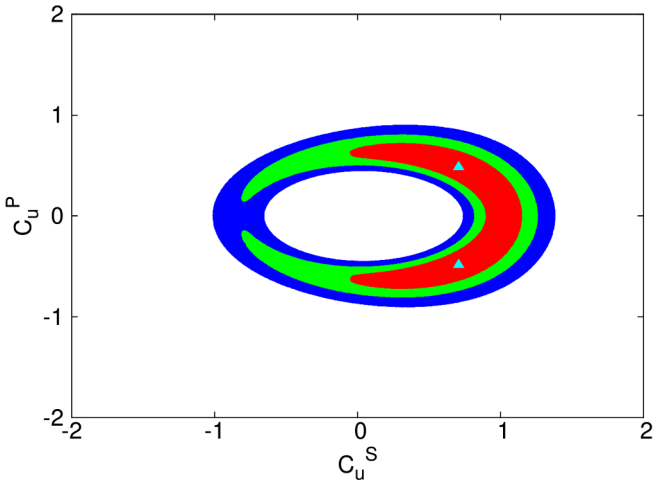

FIG. 4 (color online). The confidence-level regions of the fit by varying the scalar Yukawa couplings C_u^S and C_v, and the pseudoscalar Yukawa couplings C_u^P, while keeping others at the SM values. The description of contour regions is the same as in Fig. 2.

TABLE VII. The best-fit values and the 1σ errors for the parameters in the CP-violating fits and the corresponding chi-square after ICHEP 2014.

Cases	CPV 3		CPV 4	
Parameters	Vary C_u^S, C_u^P, C_v		Vary ΔS^γ, ΔS^g, ΔP^γ, ΔP^g	
	After ICHEP 2014			
C_u^S	$0.71^{+0.36}_{-0.46}$	$0.71^{+0.36}_{-0.46}$	1	1
C_d^S	1	1	1	1
C_ℓ^S	1	1	1	1
C_v	$0.946^{+0.084}_{-0.089}$	$0.946^{+0.084}_{-0.089}$	1	1
ΔS^γ	0	0	$0.04^{+14.69}_{-1.50}$	$7.90^{+6.84}_{-9.36}$
ΔS^g	0	0	$-0.01^{+0.05}_{-1.33}$	$-0.38^{+0.42}_{-0.96}$
$\Delta\Gamma_{\rm tot}$ (MeV)	0	0	0	0
C_u^P	$0.48^{+0.17}_{-1.14}$	$-0.48^{+1.14}_{-0.17}$	0	0
ΔP^γ	0	0	$-3.27^{+11.36}_{-4.83}$	$-7.25^{+15.35}_{-0.85}$
ΔP^g	0	0	$0.00^{+0.69}_{-0.69}$	$-0.58^{+1.27}_{-0.11}$
χ^2/d.o.f.	16.03/26	16.03/26	15.81/25	15.81/25
p value	0.935	0.935	0.920	0.920

TABLE VIII. The best-fit values and the 1σ errors for the parameters in the CP-violating fits and the corresponding chi-square after ICHEP 2014.

Cases	CPV N4	CPV N5	CPV N6	CPV N7
Parameters	Vary C_u^S, C_u^P, C_v, ΔS^γ	Vary C_u^S, C_u^P, C_v, ΔS^γ, ΔP^γ	Vary C_u^S, C_u^P, C_v, ΔS^γ, ΔP^γ, ΔS^g	Vary C_u^S, C_u^P, C_v, ΔS^γ, ΔP^γ, ΔS^g, ΔP^g
	After ICHEP 2014			
C_u^S	$1.04^{+0.10}_{-0.47}$	$1.04^{+0.10}_{-0.47}$	$1.22^{+0.32}_{-0.67}$	$1.20^{+0.33}_{-2.74}$
C_d^S	1	1	1	1
C_ℓ^S	1	1	1	1
C_v	$0.933^{+0.078}_{-0.082}$	$0.933^{+0.078}_{-0.082}$	$0.944^{+0.080}_{-0.084}$	$0.944^{+0.080}_{-0.084}$
ΔS^γ	$-1.10^{+1.19}_{-0.81}$	$-0.34^{+14.76}_{-1.57}$	$-0.44^{+15.04}_{-1.89}$	$-0.38^{+18.92}_{-1.95}$
ΔS^g	0	0	$-0.13^{+0.26}_{-1.58}$	$-0.12^{+1.91}_{-1.59}$
$\Delta\Gamma_{\rm tot}$ (MeV)	0	0	0	0
C_u^P	0.00 ± 0.56	0.00 ± 0.56	$-0.07^{+0.78}_{-0.64}$	$-0.20^{+1.74}_{-1.33}$
ΔP^γ	0	$-3.19^{+11.66}_{-5.64}$	$-3.37^{+13.03}_{-6.30}$	$-3.06^{+14.75}_{-8.63}$
ΔP^g	0	0	0	$0.26^{+2.03}_{-2.56}$
χ^2/d.o.f.	15.13/25	15.13/24	14.85/23	14.85/22
p value	0.938	0.917	0.900	0.869

B. CP violating fits

We devote this section to including the pseudoscalar top-Yukawa coupling C_u^P, and the pseudoscalar contributions ΔP^γ and ΔP^g.

1. CPV3: Vary C_u^S, C_u^P and C_v

We have shown in Ref. [3] that C_u^S and C_u^P satisfy an elliptical equation, so that the allowed regions display elliptical shapes, as shown in Fig. 4. We also find that the size of uncertainties decreases slightly, as shown in the second and third columns of Table VII.

2. CPV4: Vary ΔS^γ, ΔS^g, ΔP^γ, and ΔP^g

The result is shown in the last two columns in Table VII, and more or less similar to the result of summer 2013 [3], taking account of the large errors of ΔS^γ and ΔP^γ.

3. CPV N4: Vary C_u^S, C_u^P, C_v, ΔS^γ; CPV N5: vary C_u^S, C_u^P, C_v, ΔS^γ, ΔP^γ

The results are shown in the second and third columns of Table VIII. We observe that the pseudoscalar couplings C_u^P and ΔP^γ are consistent with zero, and thus the fits are otherwise the same as CPC N3.

TABLE IX. Degenerate chi-square minima of *CPC 6* case.

Cases	CPC 6							
Parameters	Vary C_u^S, C_d^S, C_ℓ^S, C_v, ΔS^γ, ΔS^g							
	After ICHEP 2014							
C_u^S	$1.22^{+0.32}_{-0.38}$	$1.22^{+0.32}_{-0.38}$	$1.22^{+0.32}_{-0.38}$	$1.22^{+0.32}_{-0.38}$	$1.22^{+0.32}_{-0.38}$	$1.22^{+0.32}_{-0.38}$	$1.22^{+0.32}_{-0.38}$	$1.22^{+0.32}_{-0.38}$
C_d^S	$0.97^{+0.34}_{-0.30}$	$0.97^{+0.34}_{-0.30}$	$-0.97^{+0.30}_{-0.34}$	$-0.97^{+0.30}_{-0.34}$	$0.97^{+0.34}_{-0.30}$	$0.97^{+0.34}_{-0.30}$	$-0.97^{+0.30}_{-0.34}$	$-0.97^{+0.30}_{-0.34}$
C_ℓ^S	$1.00^{+0.18}_{-0.17}$	$-1.00^{+0.17}_{-0.18}$	$1.00^{+0.18}_{-0.17}$	$-1.00^{+0.17}_{-0.18}$	$1.00^{+0.18}_{-0.17}$	$-1.00^{+0.17}_{-0.18}$	$1.00^{+0.18}_{-0.17}$	$-1.00^{+0.17}_{-0.18}$
C_v	$0.94^{+0.11}_{-0.12}$	$0.94^{+0.11}_{-0.12}$	$0.94^{+0.11}_{-0.12}$	$0.94^{+0.11}_{-0.12}$	$0.94^{+0.11}_{-0.12}$	$0.94^{+0.11}_{-0.12}$	$0.94^{+0.11}_{-0.12}$	$0.94^{+0.11}_{-0.12}$
ΔS^γ	$-1.39^{+1.02}_{-0.95}$	$-1.44^{+1.02}_{-0.95}$	$-1.43^{+1.02}_{-0.95}$	$-1.47^{+1.02}_{-0.95}$	$-1.40^{+1.02}_{-0.95}$	$-1.44^{+1.02}_{-0.95}$	$-1.43^{+1.02}_{-0.95}$	$-1.47^{+1.02}_{-0.95}$
ΔS^g	$-0.14^{+0.29}_{-0.25}$	$-0.14^{+0.29}_{-0.25}$	$-0.22^{+0.28}_{-0.24}$	$-0.22^{+0.28}_{-0.24}$	$-1.47^{+0.28}_{-0.24}$	$-1.47^{+0.28}_{-0.24}$	$-1.54^{+0.28}_{-0.25}$	$-1.54^{+0.28}_{-0.25}$
$\Delta\Gamma_{\rm tot}$ (MeV)	0	0	0	0	0	0	0	0
χ^2/d.o.f.	14.83/23	14.83/23	14.83/23	14.83/23	14.83/23	14.83/23	14.83/23	14.83/23
p value	0.901	0.901	0.901	0.901	0.901	0.901	0.901	0.901
Cases	CPC 6							
Parameters	Vary C_u^S, C_d^S, C_ℓ^S, C_v, ΔS^γ, ΔS^g							
	After ICHEP 2014							
C_u^S	$-1.23^{+0.38}_{-0.32}$	$-1.23^{+0.38}_{-0.32}$	$-1.23^{+0.38}_{-0.32}$	$-1.23^{+0.38}_{-0.32}$	$-1.23^{+0.38}_{-0.32}$	$-1.23^{+0.38}_{-0.32}$	$-1.23^{+0.38}_{-0.32}$	$-1.23^{+0.38}_{-0.32}$
C_d^S	$0.97^{+0.34}_{-0.30}$	$0.97^{+0.34}_{-0.30}$	$-0.97^{+0.30}_{-0.34}$	$-0.97^{+0.30}_{-0.34}$	$0.97^{+0.34}_{-0.30}$	$0.97^{+0.34}_{-0.30}$	$-0.97^{+0.30}_{-0.34}$	$-0.97^{+0.30}_{-0.34}$
C_ℓ^S	$1.00^{+0.18}_{-0.17}$	$-1.00^{+0.17}_{-0.18}$	$1.00^{+0.18}_{-0.17}$	$-1.00^{+0.17}_{-0.18}$	$1.00^{+0.18}_{-0.17}$	$-1.00^{+0.17}_{-0.18}$	$1.00^{+0.18}_{-0.17}$	$-1.00^{+0.17}_{-0.18}$
C_v	$0.94^{+0.11}_{-0.12}$	$0.94^{+0.11}_{-0.12}$	$0.94^{+0.11}_{-0.12}$	$0.94^{+0.11}_{-0.12}$	$0.94^{+0.11}_{-0.12}$	$0.94^{+0.11}_{-0.12}$	$0.94^{+0.11}_{-0.12}$	$0.94^{+0.11}_{-0.12}$
ΔS^γ	$2.90^{+1.11}_{-1.11}$	$2.85^{+1.11}_{-1.11}$	$2.87^{+1.12}_{-1.11}$	$2.82^{+1.12}_{-1.11}$	$2.90^{+1.11}_{-1.11}$	$2.85^{+1.11}_{-1.11}$	$2.87^{+1.12}_{-1.11}$	$2.82^{+1.11}_{-1.11}$
ΔS^g	$0.22^{+0.24}_{-0.28}$	$0.22^{+0.24}_{-0.28}$	$0.14^{+0.25}_{-0.29}$	$0.14^{+0.25}_{-0.29}$	$1.54^{+0.25}_{-0.28}$	$1.54^{+0.25}_{-0.28}$	$1.47^{+0.24}_{-0.28}$	$1.47^{+0.24}_{-0.28}$
$\Delta\Gamma_{\rm tot}$ (MeV)	0	0	0	0	0	0	0	0
χ^2/d.o.f.	14.83/23	14.83/23	14.83/23	14.83/23	14.83/23	14.83/23	14.83/23	14.83/23
p value	0.901	0.901	0.901	0.901	0.901	0.901	0.901	0.901

4. CPV N6: Vary C_u^S, C_u^P, C_v, ΔS^γ, ΔP^γ, ΔS^g; CPV N7: vary C_u^S, C_u^P, C_v, ΔS^γ, ΔP^γ, ΔS^g, ΔP^g

The results are shown in the last two columns of Table VIII. We observe that the pseudoscalar couplings C_u^P, ΔP^γ, and ΔP^g are close to zero within uncertainties, and thus the fits are otherwise the same as CPC N4.

IV. DISCUSSION

The Higgs-boson masses recorded in various channels are slightly different, roughly vary between 124.5 and 125.5 GeV. Here we shall explain the M_H dependence in calculating the signal strengths is negligible. In our approach, the theoretical signal strength is factorized into a product of

$$\hat{\mu}(\mathcal{P},\mathcal{D}) \simeq \hat{\mu}(\mathcal{P})\hat{\mu}(\mathcal{D}),$$

where $\mathcal{P}=$ ggF, VBF, VH, ttH denotes the production mechanisms and $\mathcal{D}=\gamma\gamma, ZZ, WW, b\bar{b}, \tau\bar{\tau}$ the decay channels. On the production side, the $\hat{\mu}(\mathcal{P})$ is simply given in terms of the couplings involved:

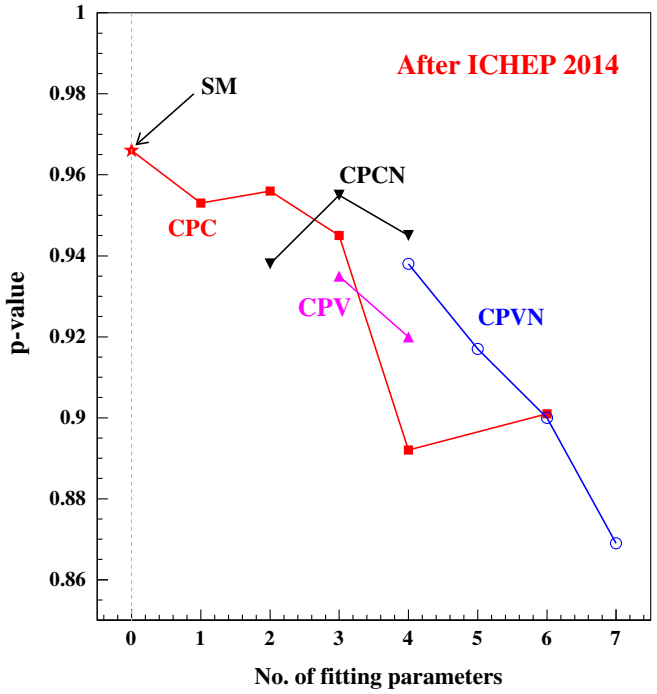

FIG. 5 (color online). The p values for various fits considered in this work, including CP-conserving (CPC) and CP-violating (CPV) ones.

$$\hat{\mu}(\text{ggF}) = \frac{|S^g(M_H)|^2 + |P^g(M_H)|^2}{|S^g_{\text{SM}}(M_H)|^2},$$
$$\hat{\mu}(\text{VBF}) = g^2_{HWW,HZZ},$$
$$\hat{\mu}(\text{VH}) = g^2_{HWW,HZZ},$$
$$\hat{\mu}(\text{ttH}) = (g^S_{H\bar{t}t})^2 + (g^P_{H\bar{t}t})^2.$$

We can easily see that the M_H dependence appears only in the loop functions of $S^g(M_H)$ and $P^g(M_H)$. We take the CPC6 fit for demonstration. We substitute the best-fit point of CPC6 into $S^g(M_H)$ and calculate the $\hat{\mu}(\text{ggF})$. We obtain $\hat{\mu}(\text{ggF}, M_H = 124.5\ \text{GeV}) = 1.014$ while $\hat{\mu}(\text{ggF}, M_H = 125.5\ \text{GeV}) = 1.016$. It is a mere 0.2% difference. Similarly, on the decay side the M_H dependence appears in the loop functions of $S^\gamma(M_H)$ and $P^\gamma(M_H)$. Again, we substitute the best-fit point of CPC6 into $S^\gamma(M_H)$ and calculate $\hat{\mu}(\gamma\gamma)$. We obtain $\hat{\mu}(\gamma\gamma, M_H = 124.5\ \text{GeV}) = 1.2203$, while $\hat{\mu}(\gamma\gamma, M_H = 125.5\ \text{GeV}) = 1.2195$. The difference is less than 0.1%. Overall, the product $\hat{\mu}(ggF) \times \hat{\mu}(\gamma\gamma)$ differs by about 0.1%. Thus, this uncertainty from different Higgs masses is far less than the uncertainties of the data on signal strengths. We can safely ignore the M_H dependence in the mass range given by data.

The most significant updates between summer 2013 and 2014 are the diphoton signal strengths reported by both ATLAS and CMS, and also the full set of data was analyzed for fermionic channels. Although more decay channels are analyzed, e.g., $WH \to 3\ell 3\nu$ and $ttH \to tt\gamma\gamma$, the uncertainties are still too large to give any impact to the fits. The p values for all the fits are plotted in Fig. 5. The SM still provides the best fit to the whole set of data and enjoys a substantial better p value than the last year.

We offer the following comments before we close:

(1) The most constrained coupling is the Higgs-gauge coupling. In various fits, it is constrained to the range 0.93–1.00 with about 7%–12% uncertainties. The uncertainties are reduced by about 10%.
(2) The CPC top-Yukawa coupling C^S_u is now more preferred to be positive in those fits with ΔS^γ and ΔS^g fixed at zero. This is because the top contribution with $C^S_u > 0$ can cancel a part of the W contribution such that the prediction is close to the SM value and thus the data.
(3) The data cannot rule out the pseudoscalar couplings, as shown in Fig. 4, and only a combination of C^S_u and C^P_u is constrained in the form of an elliptical equation.
(4) One of the most useful implications is the invisible decay branching ratio of the Higgs boson. We obtain $B(H \to \text{nonstandard}) < 19\%$.
(5) The possibility of having vanishing C^S_u has been ruled out at 68.3% C.L.

ACKNOWLEDGMENTS

This work was supported the National Science Council of Taiwan under Grants No. NSC 102-2112-M-007-015-MY3. J. S. L. was supported by the National Research Foundation of Korea (NRF) Grant No. 2013R1A2A2A01015406. This study was also financially supported by Chonnam National University, 2012. J. S. L. thanks the National Center for Theoretical Sciences (Hsinchu, Taiwan) for the great hospitality extended to him while this work was being performed.

[1] G. Aad *et al.* (ATLAS Collaboration), Phys. Lett. B **716**, 1 (2012).
[2] S. Chatrchyan *et al.* (CMS Collaboration), Phys. Lett. B **716**, 30 (2012).
[3] K. Cheung, J. S. Lee, and P.-Y. Tseng, J. High Energy Phys. 05 (2013) 134.
[4] A. Falkowski, F. Riva, and A. Urbano, J. High Energy Phys. 11 (2013) 111; J. Cao, P. Wan, J. M. Yang, and J. Zhu, J. High Energy Phys. 08 (2013) 009; P. P. Giardino, K. Kannike, I. Masina, M. Raidal, and A. Strumia, J. High Energy Phys. 05 (2014) 046; A. Djouadi and G. Moreau, Eur. Phys. J. C **73**, 2512 (2013); P. Bechtle, S. Heinemeyer, O. Stl, T. Stefaniak, and G. Weiglein, Eur. Phys. J. C **74**, 2711 (2014); G. Belanger, B. Dumont, U. Ellwanger, J. F. Gunion, and S. Kraml, Phys. Rev. D **88**, 075008 (2013); P. Artoisenet, P. de Aquino, F. Demartin, R. Frederix, S. Frixione, F. Maltoni, M. K. Mandal, P. Mathews *et al.*, J. High Energy Phys. 11 (2013) 043; S. Choi, S. Jung, and P. Ko, J. High Energy Phys. 10 (2013) 225; V. Barger, L. L. Everett, H. E. Logan, and G. Shaughnessy, Phys. Rev. D **88**, 115003 (2013); D. Lpez-Val, T. Plehn, and M. Rauch, J. High Energy Phys. 10 (2013) 134; S. Chang, S. K. Kang, J.-P. Lee, K. Y. Lee, S. C. Park, and J. Song, J. High Energy Phys. 09 (2014) 101; K. Cheung, J. S. Lee, and P.-Y. Tseng, J. High Energy Phys. 01 (2014) 085; A. Celis, V. Ilisie, and A. Pich, J. High Energy Phys. 12 (2013) 095; J. Ellis, V. Sanz, and T. You, J. High Energy Phys. 07 (2014) 036.
[5] Plenary talk by M. Kado, in Proceedings of ICHEP 2014, Spain.
[6] Plenary talk by A. David, in Proceedings of ICHEP 2014, Spain.
[7] G. Aad *et al.* (ATLAS Collaboration), arXiv:1408.7084.
[8] V. Khachatryan *et al.* (CMS Collaboration), arXiv:1407.0558.

[9] G. Aad *et al.* (ATLAS Collaboration), Phys. Rev. D **90**, 052004 (2014).
[10] S. Chatrchyan *et al.* (CMS Collaboration), Phys. Rev. D **89**, 092007 (2014).
[11] Talk by C. Mills, in Proceedings of ICHEP 2014, Spain.
[12] S. Chatrchyan *et al.* (CMS Collaboration), J. High Energy Phys. 01 (2014) 096.
[13] S. Chatrchyan *et al.* (CMS Collaboration), Phys. Rev. D **89**, 012003 (2014).
[14] S. Chatrchyan *et al.* (CMS Collaboration), J. High Energy Phys. 05 (2014) 104.
[15] Talk by E. Shabalina, in Proceedings of ICHEP 2014, Spain.
[16] The CMS Collaboration, Report No. CMS-PAS-HIG-14-010.
[17] Talk by K. Herner, in Proceedings of ICHEP 2014, Spain.
[18] The ATLAS Collaboration, Report No. ATLAS-CONF-2013-012.
[19] The CMS Collaboration, Report No. CMS PAS HIG-13-001.
[20] The ATLAS Collaboration, Report No. ATLAS-CONF-2013-034.
[21] The CMS Collaboration, Report No. CMS PAS HIG-13-002.
[22] The CMS Collaboration, Report No. CMS PAS HIG-13-003.
[23] The ATLAS Collaboration, Report No. ATLAS-CONF-2013-079.
[24] The ATLAS Collaboration, Report No. ATLAS-CONF-2013-108.
[25] A. Juste, in Proceedings of HCP2012, 15 November 2012, Kyoto, Japan, http://kds.kek.jp/conferenceDisplay.py?confId=9237.
[26] See, for example, F. Frensch (CMS) and M. Zur Nedden (ATLAS), in Proceedings of SUSY, 25 July 2014.